Algebraic Distance Field for Meshless Analysis of Free Form CAD Models

Kritika Upreti and Ganesh Subbarayan

Purdue University, ganeshs@purdue.edu

ABSTRACT

In the class of problems containing embedded boundaries, the fields approximating behavior on the boundaries are often blended with approximations built on the underlying domain using weight functions. For example, analysis of objects in which bounding surfaces are embedded into regularly structured grids, or when the boundaries are moved by the governing physics as in crack propagation or solidification problems. The blending weight functions in the approximations are typically dependent on the distance from the bounding surface. For general domains, bounded by free form curves or surfaces, the distance fields have to be constructed numerically. This may require either a polytope approximation to the boundary and/or an iterative solution to determine the exact distance to the boundary. In this paper, we describe a purely algebraic, and computationally efficient, technique for constructing distance measures as level sets from Non-Uniform Rational B-Splines (NURBS) boundaries that retain the geometric exactness of the boundaries while eliminating the need for iterative distance calculation.

Keywords: distance field, implicitization, NURBS, R-functions.
DOI: 10.3722/cadaps.2013.427-443

1 INTRODUCTION

Problems with embedded boundaries commonly occur both in analysis of solid models in which bounding surfaces are embedded in a regular grid, and in the so-called moving boundary problems. Moving boundary problems, in general, require tracking the motion of physics driven complex boundaries within the domain (Fig. 1). Boundaries of the geometric models in such problems may also evolve as a result of design intent such as in an optimal design problem. Fig. 2 summarizes the various types of boundaries that need to be modeled in engineering analysis problems. The geometrical shapes of these boundaries may be modeled either implicitly or explicitly. The computational techniques to such problems commonly rely on implicit representation of boundaries wherein the

boundary location is ὸdiffusely‘ captured using approaches such as phase-field models [4, 5, 18]. Such interface capturing schemes will require more degrees of freedom than an explicit or interface-tracking scheme [9]. Further, the local geometric properties (naturally existing tangents, normals and curvature) are often less accurate (in implicit geometries) or not uniquely defined. Also, a common challenge in implicit schemes is the numerical stability of evolution algorithms [11]. On the other hand, in an explicit technique, there always exists an accurate parametric description of the boundaries, which can be explicitly manipulated/evolved.

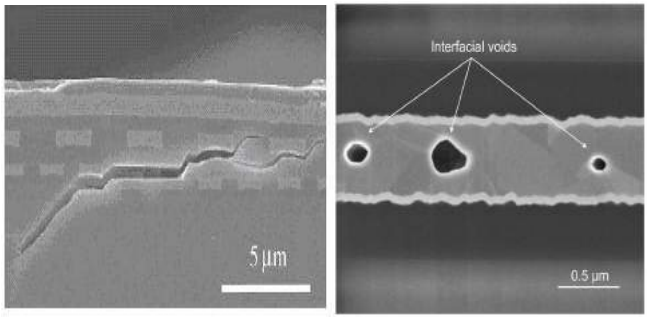

Fig. 1: Moving boundary problems: (a) Cracks in semiconductor chip dielectric stacks (adapted from [12]), and (b) Electromigration driven void growth (adapted from [22]).

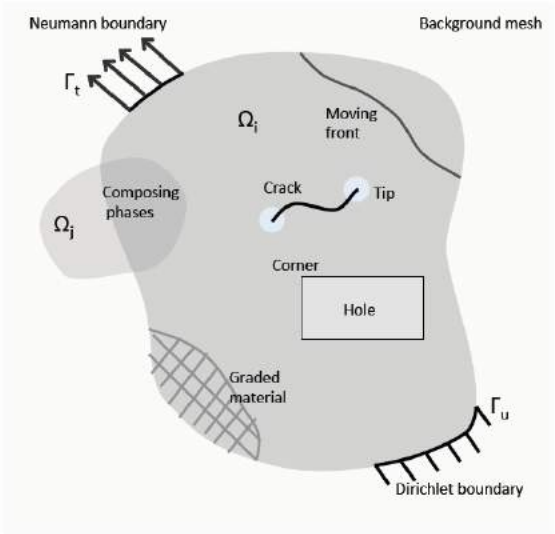

Fig. 2: Illustration of the different types of boundaries encountered in engineering analysis.

The modeling strategy adopted in this work relies on the Hierarchical Partition of Unity Field Compositions (HPFC) theory [14], which describes a complex design state (represented by a triad of *functions* describing geometry, material and behavior), through hierarchical compositions of sub-domains, with each sub-domain possessing a primitive design state. Further, the global design state is constructed through a weighted composition of primitive design states such that the weights satisfy partition of unity [1, 10] over the global domain (Fig. 3). Such partitions of unity ensure convergence of

the global approximations when errors in local approximations are bounded. The form of the constructed fields (geometry, material or behavior) is:

$$f(x) = \sum_i w^i(x) f^i(x) \tag{1.1}$$

$$\sum_i w^i(x) = 1 \tag{1.2}$$

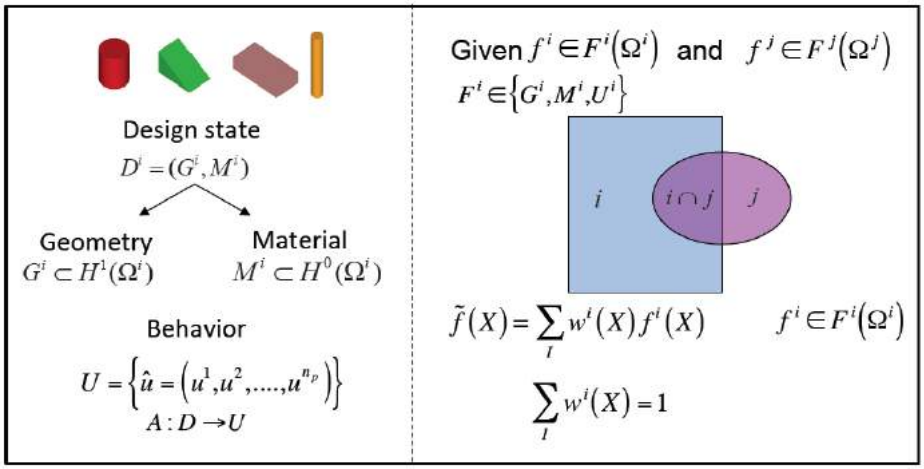

Fig. 3: The Hierarchical Partition of Unity Field Compositions theory describes a complex design state consisting of a triad of functions (belonging to an appropriate function space and) approximating geometry, material and behavior through compositions of functions defined on the primitive entities in a manner analogous to the constructive solid geometry procedure.

The HPFC theory has since been further generalized to model enrichments of one field by another defined on *lower-dimensional geometric entities* by Tambat et al. [21]. They further extended and generalized the HPFC theory to enrich the global approximations with known behavior or material property on surfaces within the domain. These enrichments enable the application of Dirichlet/Neumann boundary conditions on the boundaries of solids, as well as model displacement discontinuities caused by cracks or strain discontinuities at material interfaces in the interior of the solids. The influence of these internal and external boundaries at any point in the domain is blended using weight functions, which in turn depend on the distance from the boundaries. Hence, inexpensive distance calculations are essential for the analysis scheme to be computationally efficient. In general, the weight functions are required only to be monotonically decreasing functions of distance from the enriching boundaries, and the exact distance to a boundary is usually not necessary for analysis.

The exact distance at a point P for a parametric boundary $C(u,v)$ is defined through the following minimization problem:

$$d(P) = \inf \left\| C(u,v) - P \right\| \tag{1.3}$$

The solution for distance requires Newton-Raphson type iterative schemes that are computationally expensive for complex boundaries. The exact distance field may also not be sufficiently smooth for many engineering applications as spurious artifacts in the field may appear at points equidistant from the boundary. Other distance field computation techniques linearize geometry to avoid iterative

calculations [8]. Such techniques not only compromise the exactness of the boundary, they also do not guarantee smoothness of field due to linear approximation of the distance function. To obtain a smooth distance field, an R-function based approximate distance field construction technique was developed in reference [3]. But, this technique also relies on linearization of geometry.

The methodology proposed in this paper is based on two observations. First, the behavioral approximation constructed by weighted compositions of ‘primitive’ entities does not require exact measures of distance, and any monotonically decreasing function of distance is sufficient for analysis. Second, an algebraic representation of the boundary is more accurate than a polytope approximation, while retaining the advantage of computational efficiency. Therefore, in this paper, a purely algebraic description of distance measures as level sets from NURBS boundaries is developed, preserving the geometric exactness of the boundaries. The proposed technique overcomes the need for the iterative exact distance computations at every quadrature point during analysis while providing smoother and more robust (i.e., without artifacts of the exact) measure of distance as shown later in the paper. Further, the enriched field modeling technique [21] is extended to enable meshless analysis of B-rep CAD models using the proposed algebraic distance field.

2 ALGEBRAIC DISTANCE FIELD CONSTRUCTION

Given a NURBS curve bounding a geometric domain, an algebraic distance measure to the curve is constructed here, which is sufficiently smooth for engineering applications. The technique exploits Bezout’s resultant [17] based algebraic implicitization and R-functions [15, 19] for algebraic manipulations.

2.1 Implicitization using Bezout’s Resultant

Implicit representation of geometry is an equation of the form $f(x_1,\ldots,x_n)=0$ in n-dimensional space. In two-dimensional space, an implicit representation $f(x,y)=0$ can be obtained from a parametric curve through the process of implicitization [17], which is based on the elimination theory [6]. Elimination theory investigates the conditions under which sets of polynomials have common roots. Consider the familiar example of linear system of equations $Ax=0$, or

$$\begin{bmatrix} a_{11} & \cdots & a_{1n} \\ \vdots & \cdots & \vdots \\ a_{n1} & \cdots & a_{nn} \end{bmatrix} \begin{Bmatrix} x_1 \\ \vdots \\ x_n \end{Bmatrix} = 0 \tag{2.1}$$

This system will have a non-trivial solution if and only if the determinant of the coefficient matrix vanishes ie. $|A|=0$. Thus, resultant of a set of polynomials is an expression involving the coefficients of the polynomials such that the vanishing of the resultant is a necessary and sufficient condition for the set of polynomials to have a common non-trivial root.

Given a rational parametric curve $C(x(t),y(t),w(t))$ where $x=\frac{x(t)}{w(t)}$, $y=\frac{y(t)}{w(t)}$, two auxiliary polynomials can be formed as:

$$\begin{aligned} f(x,t) &= w(t)x - x(t) \\ g(y,t) &= w(t)y - y(t) \end{aligned} \tag{2.2}$$

By algebraic manipulation, these polynomials give rise to the following resultant system of equations $A\hat{x}=0$.

$$\begin{bmatrix} (a_n b_{n-1}) & \cdots & (a_n b_0) \\ \vdots & \cdots & \vdots \\ (a_n b_0) & \cdots & (a_1 b_0) \end{bmatrix} \begin{Bmatrix} t^{n-1} \\ \vdots \\ 1 \end{Bmatrix} = 0 \tag{2.3}$$

where $(a_i b_j) = a_i b_j - a_j b_i$, a and b are linear functions of x and y respectively. Bezout's resultant of $f(x,t)$ and $g(y,t)$ is $|A| = 0$. The resultant in this case is a polynomial in x and y, denoted here as $h(x,y)$. For the values of t for which $f = 0$ and $g = 0$, there exist points $P(x,y)$ lying on the curve $C(x(t), y(t), w(t))$ such that $h(x,y) = 0$. This is the implicit equation of the parametric curve $C(x(t), y(t), w(t))$.

2.2 Normalization

Implicitization of the constituent Bezier patches of the NURBS surfaces gives distance measures (level sets) from the boundary. Let $d(x_1,\ldots,x_n)$ be an exact distance function from a boundary defined by the implicit function $\Gamma(x_1,\ldots,x_n) = 0$. Then, this implicit function $\Gamma(d)$ is a distance measure from the boundary. Let $\hat{n}$ be the normal at the boundary. Taylor series expansion of $\Gamma(d)$ with respect to d near the boundary can be written as

$$\Gamma(d) = \Gamma(0) + \frac{\partial \Gamma}{\partial \hat{n}}(0)d + \frac{1}{2!}\frac{\partial^2 \Gamma}{\partial \hat{n}^2}(0)d^2 + \frac{1}{3!}\frac{\partial^3 \Gamma}{\partial \hat{n}^3}(0)d^3 + \ldots \tag{2.4}$$

The algebraic function $\Gamma(d)$ that gives a measure of distance from a boundary could be locally converted into a distance function by the following scaling.

$$\xi(d) = \frac{\Gamma(d)}{\frac{\partial \Gamma}{\partial \hat{n}}(0)} \tag{2.5}$$

Then, $\xi(d)$ yields a first order normalized distance function.

2.3 Boolean Compositions using R-functions

A disadvantage of the implicitized distance function is that it extends beyond the parametric range of the Bezier patch as shown in Fig. 4(b). This implies that this distance function, at a point in space, may not always correspond to the shortest distance to the Bezier patch.

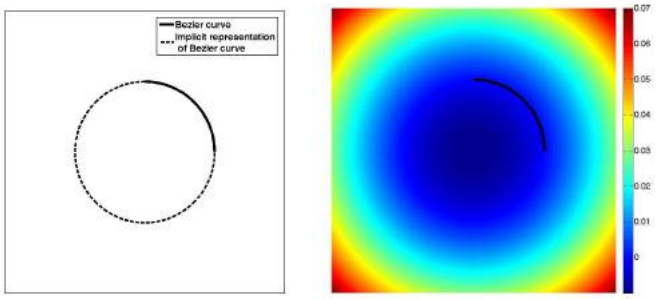

Fig. 4: Implicitized distance function: (a) An example of a Bezier curve and the corresponding implicit representation, and (b) Implicit representation does not give a distance measure from the Bezier curve.

Hence, a sequence of Boolean operations (described below) is performed between the convex hull $\phi \geq 0$ of the control polygon of the Bezier patch and the implicitized distance function $f = 0$ as shown in Fig. 5 to obtain the algebraic distance function $g = 0$ for a Bezier patch.

$$\begin{aligned} \phi_1 &= \phi \wedge f \\ \phi_2 &= \phi \wedge \sim f \\ g &= \phi_1 \wedge \phi_2 \end{aligned} \tag{2.6}$$

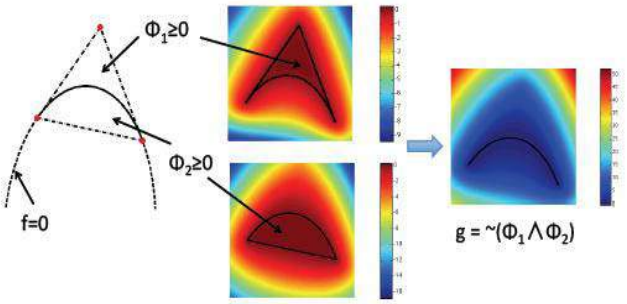

Fig. 5: Illustration of Boolean operations between the implicit function of Bezier curve and convex hull of Bezier control polygon (Note that ~ operator is applied only to change sign of the distance field g for plotting purposes and has no effect on the absolute value of the distance field).

The theory of R-functions [15, 19] provides smooth functional equivalents of Boolean operations and is therefore appropriate in an algebraic procedure. Hence, R-functions are chosen here to enable Boolean operations on functional descriptions of domains and obtain desired smoothness in the composed field. The function equivalent of the set-theoretic intersection of two functions ϕ_1 and ϕ_2 is the R-conjunction operation given by

$$\phi_1 \wedge \phi_2 = \phi_1 + \phi_2 - \sqrt{\phi_1^2 + \phi_2^2} \tag{2.7}$$

Further compositions are then carried out between adjoining Bezier patches using the R-disjunction or union operations as shown in Fig. 6(d). The R-disjunction operation is given by

$$\phi_1 \vee \phi_2 = \phi_1 + \phi_2 + \sqrt{\phi_1^2 + \phi_2^2} \tag{2.8}$$

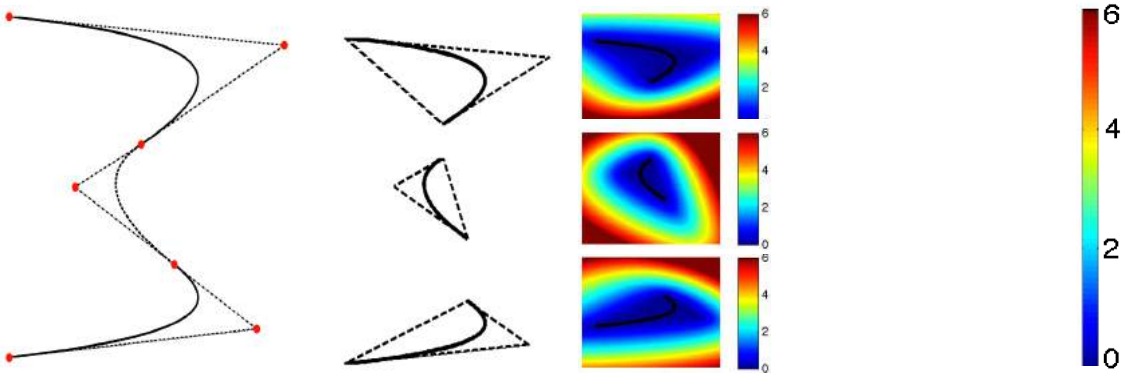

Fig. 6: Algebraic distance field construction: (a) Degree two NURBS curve with control polygon, (b) Bezier curves with respective convex hulls, (c) Distance field of each Bezier curve, and (d) Composed distance field of the NURBS curve.

Exact distance field and Algebraic distance field for a S-shaped curve are compared in Fig. 7. The encircled regions in the exact distance field are locations of spurious artifacts that occur at points equidistant from the curve. The algebraic distance field, on the other hand, gives smoother approximate distance to the curve.

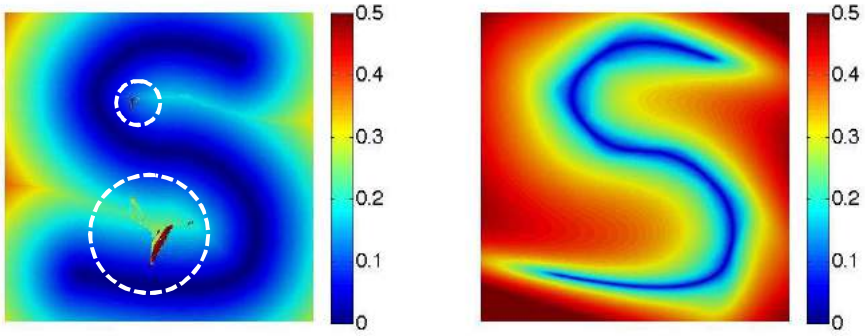

Fig. 7: Comparison of distance fields: (a) Exact distance field with spurious artifacts, (b) Algebraic distance field.

2.4 Sign Calculation for Closed Geometries

For closed curves, sign of the distance field is calculated as a by-product of the proposed technique. A bounding box is first constructed from the convex hull of the control polygon of Bezier segments. The solid edges of the convex hulls in Fig. 8(a) contribute towards constructing the bounding box while the dashed edges are removed. In this way, the bounding box encloses two types of regions as illustrated in Fig. 8(b). One is the region enclosed by the NURBS curve; the other type of region is referred to as curved Bezier polygon in this paper. Curved Bezier polygon is defined as a region bounded by a Bezier curve and a set of linear edges. Each shaded region in Fig. 8(b) is a curved Bezier polygon, same as ϕ_1 or ϕ_2 in Fig. 5 obtained by the Boolean operations between implicitized distance function f and the convex hull ϕ in Eqn. (2.6).

Fig. 8: Signed distance field: (a) Bounding box construction, (b) Shaded regions represent curved Bezier polygons, and (c) Signed field of the closed geometry.

Let P_i be a point in the plane and $g(x,y)$ be the distance field of the closed NURBS curve with bounding box field $\phi(x,y)$ and m curved Bezier polygons (Fig. 8(b)) with distance fields $\Psi_j,\ j \in 1,\ldots,m$. The sign of $\phi(x,y)$ is calculated by a point in polygon test [7]. The signed field $\Psi_j,\ j \in 1,\ldots,m$ is constructed as a by-product of the Boolean operations in Eqn. (2.6). It is equal to either $\phi_1(x,y)$ or $\phi_2(x,y)$ whichever corresponds to the shaded region in Fig. 8(b). A test vertex of the convex hull ϕ that does not lie on the Bezier curve is used to choose the right curved polygon. The test vertex must lie on the bounding box. Then, the correct curved polygon (ϕ_1 or ϕ_2) is the one for which the corresponding field value ($\phi_1(x,y)$ or $\phi_2(x,y)$) is zero at this test point. The sign of $g(x,y)$ (Fig. 8(c)) at the point P_i is given by the following scheme.

$$\text{sign}(g) = \begin{cases} -1 & \text{if } (\phi < 0) \text{ or } (\phi \geq 0 \text{ and } \Psi_j \geq 0,\ j \in 1,\ldots,m \text{ and } \mathrm{g} \neq 0), \\ 0 & \text{if } \mathrm{g} = 0, \\ 1 & \text{otherwise} \end{cases} \tag{2.9}$$

3 MESHLESS ANALYSIS TECHNIQUE USING ALGEBRAIC DISTANCE FIELD

The analysis technique developed here is based on the hierarchical partition of unity field compositions (HPFC) theory as well as its generalization to enriched field modeling developed in the references [14, 20, 21]. In this paper, the HPFC theory is further applied to construct approximations by weighted compositions of the moving boundaries with the underlying domain.

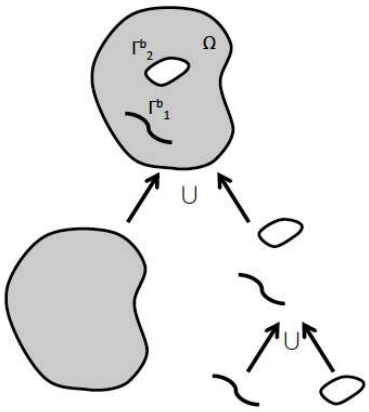

Fig. 9: Global approximation constructed by hierarchical composition of lower order boundaries with higher order primitive.

Let the geometry of the underlying domain Ω be defined as $S_\Omega(p,q,r)$ and the behavioral field as $f_\Omega(\mathbf{x}(p,q,r))$. Let the geometry of the moving boundary Γ or lower order primitive be defined

parametrically as $C_\Gamma(s,t)$ and the behavioral field as $f_\Gamma^b(\mathbf{x}(p,q,r) \rightarrow (\mathrm{s,t}))$. Then, the global approximation field $f(\mathbf{x})$ at any point $\mathbf{x}$ in the domain is given by the following weighted composition (Fig. 9).

$$f(\mathbf{x}) = w_\Omega(\mathbf{x}) f_\Omega(\mathbf{x}(p,q,r)) + w_\Omega^b(\mathbf{x}) f_\Gamma^b(\mathbf{x}(p,q,r) \rightarrow (\mathrm{s,t})) \tag{3.1}$$

Here, the weights w_Ω and w_Ω^b obey the partition of unity property [1] such that $w_\Omega + w_\Omega^b = 1$. The influence of the boundary on the underlying domain is modeled using weight field w_Ω^b constructed as a monotonically decreasing function of the algebraic distance field. Some possible functions for weight field w_Ω^b include the exponential function (Eqn. (3.2)) and the spline function (Eqn. (3.3)) [2]

$$w_\Omega^b = w_\Gamma e^{-(\frac{d}{d_e})^2} \tag{3.2}$$

$$w_\Omega^b = \begin{cases} w_\Gamma(1 - \frac{6}{8}(\frac{d}{d_s})^2 + \frac{1}{8}(\frac{d}{d_s})^3) & 0 \le \frac{d}{d_s} < 1 \\ w_\Gamma(\frac{3}{8}(2 - \frac{d}{d_s})^3) & 1 \le \frac{d}{d_s} < 2 \\ 0 & \frac{d}{d_s} \ge 2 \end{cases} \tag{3.3}$$

where, d is the algebraic distance measure from the boundary, d_e and d_s are scaling factors and w_Γ is the assigned weight value at the boundary.

In the present paper, the field approximations over the domain as well as the lower order boundaries are constructed using the NURBS basis functions. Thus, the behavioral field f_Ω is defined as

$$f_\Omega(\mathbf{x}(p,q,r)) = \sum_I N_I(p,q,r) \hat{\boldsymbol{u}}_I \tag{3.4}$$

where $N_I(p,q,r)$ are the NURBS basis functions over the underlying domain and $\hat{\boldsymbol{u}}_I$ is the field value at the *I-th* control point of the NURBS geometric domain. The behavioral field f_Γ^b is defined as

$$f_\Gamma^b(\mathbf{x}(p,q,r) \rightarrow (\mathrm{s,t})) = \sum_J N_J(s,t) \hat{\boldsymbol{v}}_J \tag{3.5}$$

where, $N_J(s,t)$ are NURBS basis functions over the lower order primitive and $\hat{\boldsymbol{v}}_J$ is the field value at the *J-th* control point of the NURBS boundary, $\mathbf{x}(p,q,r) \rightarrow (\mathrm{s,t})$ is a projection from the point $\mathbf{x}$ on the underlying domain to the closest point *P(s,t)* on the lower order primitive.

4 NUMERICAL IMPLEMENTATION

In this paper, the developed analysis technique has been applied for solving linear elasticity problems with boundary representation (B-rep) of the CAD models. The boundary conditions on the CAD model are represented as lower order primitives and composed with the approximations on the underlying domain through weight fields constructed using the algebraic distance function. The construction of discretized solution system is briefly described for such problems and the adaptive quadrature scheme used for numerical integration of stiffness matrices is discussed.

4.1 Formulation of Discretized Solution System

Consider the domain Ω with boundary Γ. The boundary Γ consists of the displacement and traction boundary conditions. The corresponding Dirichlet boundary Γ_u, or traction boundary Γ_t is modeled explicitly as lower order NURBS primitive. In general, the total potential energy for linear elastic systems is given by

$$\Pi^*(\boldsymbol{u}) = \int_\Omega \frac{1}{2}\sigma_{ij}\varepsilon_{ij}d\Omega - \int_\Omega \hat{b}_i u_i d\Omega - \int_{\Gamma_t} \hat{t}_i u_i d\Gamma \tag{4.1}$$

where, $\sigma_{ij} = D_{ijkl}\varepsilon_{kl}$ is the generalized Hooke's law relating stress σ_{ij} to strain ε_{kl}, and D_{ijkl} is the fourth order elasticity tensor. The displacement field $\boldsymbol{u}_i$ is approximated by the weighted composition between the domain and the boundary as described in Eqn. (3.1).

$$u_i = w_i^d u_i^d + w_i^b u_i^b = \tilde{u}_i^d + \tilde{u}_i^b \tag{4.2}$$

such that $w_i^d + w_i^b = 1$. Superscripts d and b correspond to domain and boundary respectively. The strain and stress components in terms of the domain and boundary displacements are as follows

$$\varepsilon_{ij} = \frac{u_{i,j} + u_{j,i}}{2} = \frac{(w^d u^d)_{i,j} + (w^d u^d)_{j,i}}{2} + \frac{(w^b u^b)_{i,j} + (w^b u^b)_{j,i}}{2} = \tilde{\varepsilon}_{ij}^d + \tilde{\varepsilon}_{ij}^b \tag{4.3}$$

$$\sigma_{ij} = D_{ijkl}\varepsilon_{kl} = D_{ijkl}\tilde{\varepsilon}_{kl}^d + D_{ijkl}\tilde{\varepsilon}_{kl}^b \tag{4.4}$$

The total potential energy is then written as a function of $\boldsymbol{u^d}$ *and* $\boldsymbol{u^b}$.

$$\Pi^*(\boldsymbol{u}^d, \boldsymbol{u}^b) = \int_\Omega \frac{1}{2}\sigma_{ij}\tilde{\varepsilon}_{ij}^d d\Omega + \int_\Omega \frac{1}{2}\sigma_{ij}\tilde{\varepsilon}_{ij}^b d\Omega - \int_\Omega \hat{b}_i \tilde{u}_i^d d\Omega - \int_\Omega \hat{b}_i \tilde{u}_i^b d\Omega - \int_{\Gamma_t} \hat{t}_i \tilde{u}_i^d d\Gamma - \int_{\Gamma_t} \hat{t}_i \tilde{u}_i^b d\Gamma \tag{4.5}$$

The stationarity of the total potential energy with respect to $\boldsymbol{u^d}$ *and* $\boldsymbol{u^b}$ yields the following equilibrium conditions.

$$\begin{aligned}
\delta\Pi^*_{\boldsymbol{u}^d} &= \int_\Omega \sigma_{ij}\,\delta\tilde{\varepsilon}_{ij}^d\, d\Omega - \int_\Omega \hat{b}_i \delta\tilde{u}_i^d d\Omega - \int_{\Gamma_t} \hat{t}_i\, \delta\tilde{u}_i^d d\Gamma = 0 \\
\delta\Pi^*_{\boldsymbol{u}^b} &= \int_\Omega \sigma_{ij}\,\delta\tilde{\varepsilon}_{ij}^b\, d\Omega - \int_\Omega \hat{b}_i \delta\tilde{u}_i^b d\Omega - \int_{\Gamma_t} \hat{t}_i\, \delta\tilde{u}_i^b d\Gamma = 0
\end{aligned} \tag{4.6}$$

$$\begin{aligned}
\delta\Pi^*_{\boldsymbol{u}^d} &= \int_\Omega D_{ijkl}\tilde{\varepsilon}_{kl}^d \delta\tilde{\varepsilon}_{ij}^d d\Omega + \int_\Omega D_{ijkl}\tilde{\varepsilon}_{kl}^b \delta\tilde{\varepsilon}_{ij}^d d\Omega - \int_\Omega \hat{b}_i \delta\tilde{u}_i^d d\Omega - \int_{\Gamma_t} \hat{t}_i\, \delta\tilde{u}_i^d d\Gamma = 0 \\
\delta\Pi^*_{\boldsymbol{u}^b} &= \int_\Omega D_{ijkl}\tilde{\varepsilon}_{kl}^d\, \delta\tilde{\varepsilon}_{ij}^b\, d\Omega + \int_\Omega D_{ijkl}\tilde{\varepsilon}_{kl}^b\, \delta\tilde{\varepsilon}_{ij}^b\, d\Omega - \int_\Omega \hat{b}_i \delta\tilde{u}_i^b d\Omega - \int_{\Gamma_t} \hat{t}_i\, \delta\tilde{u}_i^b d\Gamma = 0
\end{aligned} \tag{4.7}$$

The displacement fields of the higher and lower order primitives are next discretized using NURBS basis functions as shown in Eqns. (3.4) and (3.5).

$$\tilde{\boldsymbol{u}}^d = \boldsymbol{w}^d \sum_I N_I(p,q,r)\boldsymbol{u}_I^d = \sum_I \tilde{N}_I(p,q,r)\boldsymbol{u}_I^d \tag{4.8}$$

$$\tilde{\boldsymbol{u}}^b(\mathbf{x}(p,q,r) \to (\mathrm{s},\mathrm{t})) = \boldsymbol{w}^b \sum_J N_J(s,t)\boldsymbol{u}_J^b = \sum_J \tilde{N}_J(s,t)\boldsymbol{u}_J^b \tag{4.9}$$

After substituting the approximating fields into the equilibrium equations, the following matrix system is obtained:

$$\begin{bmatrix} K^{dd} & K^{db} \\ K^{db^T} & K^{bb} \end{bmatrix} \begin{Bmatrix} \hat{u}^d \\ \hat{u}^b \end{Bmatrix} = \begin{Bmatrix} g^d \\ g^b \end{Bmatrix} + \begin{Bmatrix} h^d \\ h^b \end{Bmatrix} \tag{4.10}$$

where, the stiffness matrices are constructed as

$$\begin{aligned} [K^{dd}] &= \int_{\Omega} (\tilde{B}^d)^T D \tilde{B}^d d\Omega \\ [K^{bb}] &= \int_{\Omega} (\tilde{B}^b)^T D \tilde{B}^b d\Omega \\ [K^{db}] &= \int_{\Omega} (\tilde{B}^d)^T D \tilde{B}^b d\Omega \end{aligned} \tag{4.11}$$

,the work equivalent forces are determined by integration of tractions on primitive boundaries

$$\begin{aligned} \{g^d\} &= \int_{\Gamma_t^d} (\tilde{N}^d)^T \hat{t} d\Gamma \\ \{g^b\} &= \int_{\Gamma_t^b} (\tilde{N}^b)^T \hat{t} d\Gamma \end{aligned} \tag{4.12}$$

and the body forces are determined as follows

$$\begin{aligned} \{h^d\} &= \int_{\Omega} (\tilde{N}^d)^T \hat{b} d\Omega \\ \{h^b\} &= \int_{\Omega} (\tilde{N}^b)^T \hat{b} d\Omega \end{aligned} \tag{4.13}$$

If Γ_b is a traction boundary, then the matrix system reduces to

$$\begin{bmatrix} K^{dd} & K^{db} \\ K^{db^T} & K^{bb} \end{bmatrix} \begin{Bmatrix} \hat{u}^d \\ \hat{u}^b \end{Bmatrix} = \begin{Bmatrix} 0 \\ g^b \end{Bmatrix} + \begin{Bmatrix} h^d \\ h^b \end{Bmatrix} \tag{4.14}$$

since $\boldsymbol{w}^d$=0 on Γ_t^d

If Γ_b is a Dirichlet boundary, then the matrix system reduces to

$$[K^{dd}]\{\hat{u}^d\} = \{g^d\} + \{h^d\} - [K^{db}]\{\hat{u}^b\} \tag{4.15}$$

since $\{\hat{u}^b\}$ are known displacements on the boundary.

For more than two primitives, the solution system is formed by a pairwise interaction between the primitives following an approach similar to that described in reference [14].

4.2 Numerical Integration

An adaptive quadrature scheme [23] developed earlier is used to accurately take into account the influence of the internal boundaries on the underlying NURBS control grid. In the implemented quadrature scheme, the parametric space of the NURBS geometry of the domain naturally forms the quadrature cells. Further, a quad-tree algorithm as shown in Fig. 10 is used to adaptively subdivide the integration cells that are intersected by internal boundaries. Point containment based on the proposed signed field is used in the quadrature scheme to ignore quadrature points that do not lie inside the material domain of the CAD model.

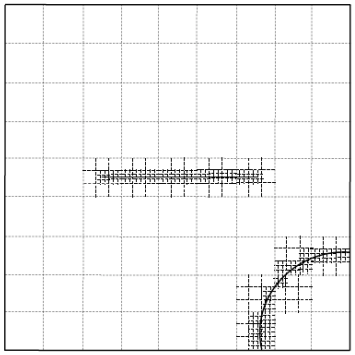

Fig. 10: Illustration of adaptive quadrature scheme for a domain with internal boundaries

5 NUMERICAL EXAMPLES

In this section, the analysis technique described in Sections 3 and 4 is applied to some elasticity problems with known analytical solutions to validate the scheme. In all of the examples, meshless analysis of B-rep CAD models is demonstrated. It is assumed that the geometric models are represented only by NURBS boundaries and that a parametric description of the domain of analysis is not available. A background mesh is constructed in each problem using a rectangular NURBS primitive. The geometric model does not conform to the background mesh. Boundary conditions are defined on the explicitly modeled lower order NURBS primitives. Weight fields are constructed using the exponential function given in Eqn. (3.2). Algebraic distances are computed from the boundaries of the lower order primitives. Material assignment is based on point containment checks using the signed field from the boundaries of the geometric model. Thus, the proposed technique allows direct analysis on B-rep CAD models without tedious mesh generation.

5.1 Plate with an Elliptical Hole

An elastic plate with an elliptical hole under uniform tension is known to have an analytical stress concentration factor that is dependent on the ratio of the major to minor diameter of the ellipse. The geometry and boundary conditions for this problem are shown in Fig. 11(a). The modulus of elasticity of the plate is assumed to be 100 units and the Poisson's ratio is 0.3. A background mesh is constructed as a rectangular ($2l$ X $2w$) NURBS primitive with the dimensions indicated in Fig. 11. The two traction boundaries are modeled explicitly as lower order NURBS primitives. The geometric model and the background mesh are independent of each other as shown in Fig. 11(b). Point containment checks in the B-rep CAD model of the plate with elliptical hole were used to eliminate quadrature points on the mesh lying outside the material domain.

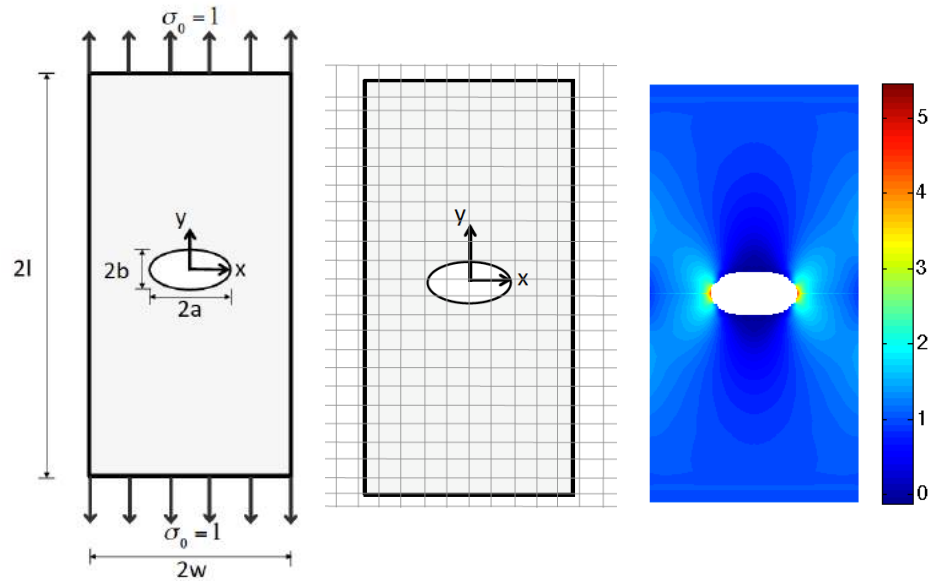

Fig. 11: Plate with elliptical hole: (a) Geometry (a = 0.2, b = 0.1, w = 0.5, l = 1) and boundary conditions, (b) Underlying control point grid is independent of the geometry, and (c) Stress plot in y-direction (σ_{yy}).

The analytical stress concentration factor for elliptical hole with $\frac{a}{b} = 2$ accounting for the finite plate width is 5.9 [13]. The stress plot (σ_{yy}) is shown in Fig.11(c) for a uniform control point grid spacing of h = 0.03 units and local refinement around the hole. The stress concentration factor obtained was 5.5292. Further local refinement resulted in an improved stress concentration factor of 5.7348.

5.2 Curved Cantilever Beam under Tip Loading

In this example, a curved cantilever beam is subjected to tip loading as shown in Fig. 12(a). The modulus of elasticity of the beam was assumed to be 100 units and the Poisson's ratio was 0.3. The analytical stress field solution is given by the following equations [16]:

$$\begin{aligned}
\sigma_r &= \frac{P}{N}(r + \frac{a^2b^2}{r^3} - \frac{a^2+b^2}{r})\sin\theta \\
\sigma_\theta &= \frac{P}{N}(3r - \frac{a^2b^2}{r^3} - \frac{a^2+b^2}{r})\sin\theta \\
\tau_{r\theta} &= -\frac{P}{N}(r + \frac{a^2b^2}{r^3} - \frac{a^2+b^2}{r})\cos\theta \\
\text{where } N &= a^2 - b^2 + (a^2+b^2)\log(\frac{b}{a})
\end{aligned} \tag{5.1}$$

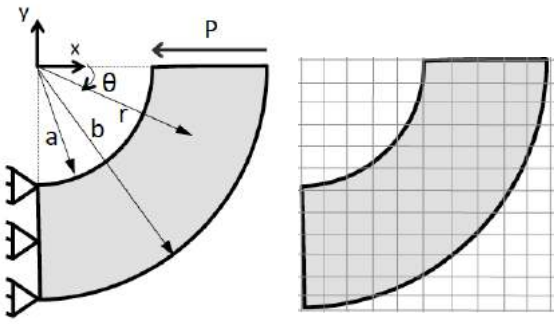

Fig. 12: Curved cantilever beam: (a) Geometry (a = 0.2, b = 0.4) and boundary conditions (P = 0.2 units), and (b) Underlying control point grid is independent of the geometry.

A background mesh was constructed as a rectangular (2b X2b) NURBS primitive with the specific numerical values as indicated in Fig. 12. The displacement and traction boundary conditions were modeled explicitly as lower order NURBS primitives. The geometric model and the background mesh are independent of each other as shown in Fig. 12(b). The variation of the numerical solution of stress field σ_θ is plotted with radial distance at $\theta = \frac{\pi}{2}$ and compared with the analytical solution in Fig. 13.

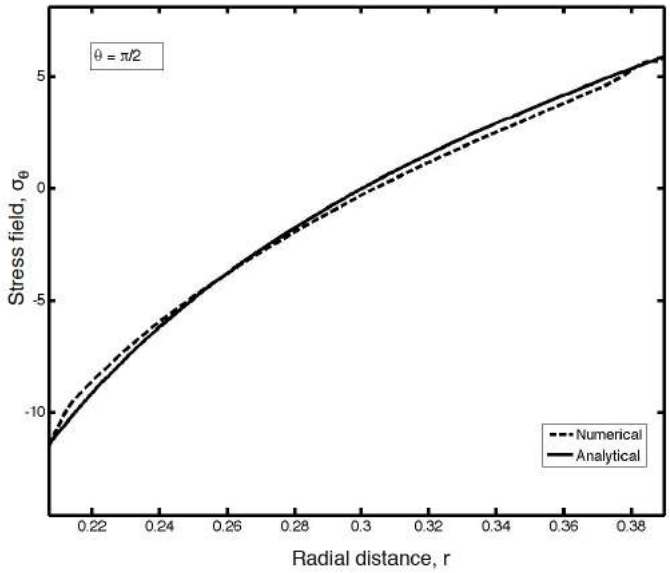

Fig. 13: Variation of stress field σ_θ with radial distance r at $\theta = \frac{\pi}{2}$.

5.3 Analysis of a Wrench under Use Load

A problem with relatively complex two-dimensional geometry is considered next; a wrench is analyzed under the loading and boundary conditions shown in Fig. 14(a). A rectangular background mesh was constructed independent of the wrench geometry as shown in Fig. 14(b). The modulus of elasticity of the wrench was assumed to be 100 units and the Poisson's ratio was 0.3. The displacement and

traction boundary conditions were modeled explicitly as lower order NURBS primitives. Weight fields were constructed from each of these primitives using the algebraic distance field measure. The effective weight field corresponding to the rectangular domain NURBS primitive in the analysis problem is shown in Fig. 15(a). Deformed shape is plotted in Fig. 15(b).

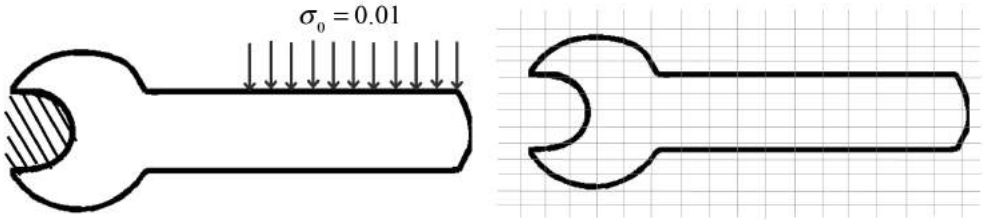

Fig. 14: Analysis using boundary representation of a wrench: (a) Loading and boundary condition on the wrench, (b) Underlying control point grid is independent of the geometry.

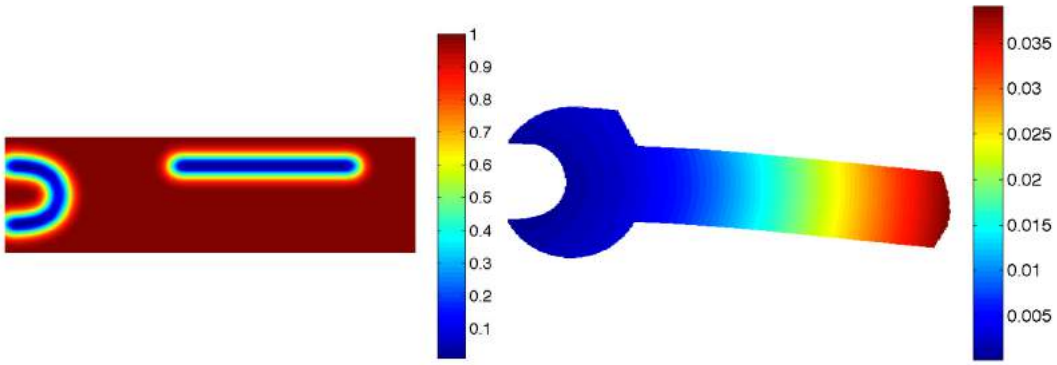

Fig. 15: Analysis results: (a) Weight field of the rectangular domain NURBS primitive constructed using algebraic distance from the displacement and traction boundaries, (b) The resultant displacement as well as the deformed shape shown magnified five times.

These examples demonstrate analysis of two-dimensional B-rep CAD models without the need for mesh generation in the domain. While the theoretical development of the algebraic distance field and the proposed meshless analysis technique for B-rep CAD models is general, an extension of this work to three-dimensions is in progress and will be reported shortly.

6 SUMMARY

In this work, a purely algebraic technique for estimating distance fields from boundaries (both internal and external) was developed. The proposed technique preserves the geometric exactness of the NURBS boundaries, and eliminates the iterative solution required of exact distance calculation. The technique enables explicit modeling of boundaries with geometric independence from the underlying domain. The fields on the boundaries are blended using weight functions with approximations built on the underlying domain while obeying the partition of unity requirement for the composed approximation. Weight functions depend on distance measures from the boundaries. The proposed algebraic distance field technique enables inexpensive distance computations at every quadrature point. It is recognized that the resultant obtained by algebraic implicitization is a distance measure. The algorithmic development of the algebraic distance field from the resultant based implicit function is discussed

using normalization techniques and Boolean compositions. Also, algorithms for construction of signed distance measures for bounded domains are presented. The signed distance field enables inexpensive point-containment checks for complex geometries. Analysis of B-rep CAD models has been demonstrated without the need of mesh generation in the domain.

REFERENCES

[1] Babuǵka, I.; Melenk, J.M.: The Partition of Unity Method, International Journal for Numerical Methods in Engineering 40 (4) (1997) 727ð758. http://dx.doi.org/10.1002/(SICI)1097-0207(19970228)40:4<727::AID-NME86>3.0.CO;2-N

[2] Belytschko, T.; Krongauz, Y.; Organ, D.; Fleming, M.; Krysl, P.: Meshless methods: An overview and recent developments, Computer Methods in Applied Mechanics and Engineering 7815 (96).

[3] Biswas, A.; Shapiro, V.: Approximate distance fields with non-vanishing gradients, Graphical Models 66 (2004) 133-159. http://dx.doi.org/10.1016/j.gmod.2004.01.003

[4] Chen, L.-Q.: Phase-Field Models for Microstructure Evolution, Annual Review of Materials Research, 32(1), (2002) Aug., pp. 113ð140.

[5] Chessa, J.; Smolinski, P.; Belytschko, T.: The extended finite element method (xfem) for solidification problems, International Journal for Numerical Methods in Engineering 53 (8) (2002) 1959ð1977. http://dx.doi.org/10.1002/nme.386

[6] Dixon, A.: The eliminant of three quantics in two independent variables, Proceedings of the London Mathematical Society 2 (1) (1909) 49. http://dx.doi.org/10.1112/plms/s2-7.1.49

[7] Feito, F.; Torres, J.; Urena, A.: Orientation, simplicity, and inclusion test for planar polygons, Computers & Graphics 19 (4) (1995) 595-600. http://dx.doi.org/10.1016/0097-8493(95)00037-D

[8] Jones, M.W.; Baerentzen, J.A.; Sramek, M.: 3D distance fields: a survey of techniques and applications., IEEE transactions on visualization and computer graphics 12 (4) (2006) 581{99. doi:10.1109/TVCG.2006.56.

[9] Li, B.; Lowengrub, J.; Ratz, A.; Voigt, A.: Geometric evolution laws for thin crystalline films: modeling and numerics, Communications in Computational Physics 6 (3) (Sept. 2009) 433 ð 82.

[10] Melenk, J.M.; Babuǵka, I.: The partition of unity finite element method: Basic theory and applications, Computer Methods in Applied Mechanics and Engineering, Volume 139, Issues 1ð4, 15 December 1996, Pages 289-314, ISSN 0045-7825, 10.1016/S0045-7825(96)01087-0.

[11] Mysore, K.; Morgan, O.; Subbarayan, G.: NURBS representational strategies for tracking moving boundaries and topological changes during phase evolution, Computer Methods in Applied Mechanics and Engineering 200 (33-36) (2011) 2594ð2610. http://dx.doi.org/10.1016/j.cma.2011.04.002

[12] Ocaña, I.; Molina-Aldareguia, J.M.; Gonzalez, D.; Elizalde, M.R.; Sánchez, J.M.; Martínez-Esnaola, J.M.; Gil Sevillano, J.; Scherban, T.; Pantuso, D.; Sun, B.; Xu, G.; Miner, B.; He, J.; Maiz, J.: Fracture characterization in patterned thin films by cross-sectional nanoindentation, Acta Materialia, Volume 54, Issue 13, August 2006, Pages 3453-3462, ISSN 1359-6454, 10.1016/j.actamat.2006.03.027.

[13] Pilkey, W. D.: Peterson's Stress Concentration Factors, Second Edition, New York: Wiley-Interscience, 1997. http://dx.doi.org/10.1002/9780470172674

[14] Rayasam, M; Srinivasan, V; Subbarayan, G: CAD Inspired Hierarchical Partition of Unity Constructions for NURBS-based Meshless Design, Analysis and Optimization, International Journal for Numerical Methods in Engineering, vol. 72, pp. 1452-1489, 2007. http://dx.doi.org/10.1002/nme.2046

[15] Rvachev, V.L.; Shieko, T.I.: R-functions in boundary value problems in mechanics, Applied Mechanics Reviews 1995; 48:151ð188.17.
[16] Sadd, M.H.: Elasticity Theory, Applications, and Numerics. 2005, Burlington, MA: Elsevier Butterworth-Heinemann.
[17] Sederberg, T.W.; Anderson, D.C.; Goldman, R.N.: Implicit Representation of Parametric Curves and Surfaces, Computer Vision, Graphics and Image Processing, 28:72ð84, 1984 http://dx.doi.org/10.1016/0734-189X(84)90140-3
[18] Shapiro, V.; Tsukanov, I.: Meshfree simulation of deforming domains, Computer-Aided Design 1999; 31:459ð471.18.
[19] Shapiro, V.: Theory of R-functions and applications: a primer, CPA Technical Report CPA88-3, Cornell Programmable Automation. Sibley School of Mechanical Engineering, Ithaca, NY, 1998.
[20] Srinivasan, V.; Subbarayan, G.: Hierarchical partition of unity field compositions (HPFC) for optimal design in presence of cracks, Mechanics of Advanced Materials and Structures 17 (2010) 467-480. http://dx.doi.org/10.1080/15376494.2010.508989
[21] Tambat, A.; Subbarayan, G.: Explicit Geometry-Based Isogeometric Enriched Field Approximations, under review in Computational Methods in Applied Mechanics and Engineering.
[22] Tan, C.S.; Reif, R.; Theodore, N.D.; Pozder, S.: Observation of interfacial void formation in bonded copper layers, Applied Physics Letters, 87:201909, 2005. http://dx.doi.org/10.1063/1.2130534
[23] Zhang, X.; Rayasam, M.; Subbarayan, G.: A meshless, compositional approach to shape optimal design, Computer Methods in Applied Mechanics and Engineering, Volume 196, Issues 17ð20, 15 March 2007, Pages 2130-2146, ISSN 0045-7825, 10.1016/j.cma.2006.11.008.